PNAS RESEARCH ARTICLE | CHEMISTRY CELL BIOLOGY OPEN ACCESS

Optimizing mRNA delivery with targeted elastin-like polypeptide–based LENN formulations: Insights into the endocytosis mechanism

Saloni Darji[a,b], Feng Qu[a,b], Marissa Henager[a,b], Ankita Prasad[a], Bennett D. Elzey[b,c], Christina R. Ferreira[b], and David H. Thompson[a,1]

Affiliations are included on p. 11.

Edited by Joseph DeSimone, Stanford University, Stanford, CA; received February 3, 2025; accepted November 11, 2025

Gene delivery has emerged as a groundbreaking technique for altering gene expression, offering new possibilities in treating a vast array of diseases. We report a layer-by-layer elastin-like polypeptide nucleic acid nanoparticle (LENN) system for mRNA delivery as an attractive alternative to viral vectors and lipid nanoparticle (LNP) systems. This study focuses on determining the physical characteristics of LENN bearing mRNA cargo and assessing their biological performance in T24 bladder tumor cells. Our data show that mRNA encoding luciferase forms stable 30 to 130 nm LENN particles via batch mixing to efficiently encapsulate the mRNA strands, are resistant to heparin challenge, and are capable of storage at −20 °C for 3 d as lyophilized powders while retaining full biological activity after rehydration. We also demonstrate that LENN targeted to the epidermal growth factor receptor (EGFR) can efficiently deliver the mRNA cargo to the cytosol of EGFR+ T24 human bladder cancer cells via clathrin-mediated endocytosis where it is translationally active. Lipid profiling analyses show the significant role that upregulated phospholipid biosynthesis plays in nanoparticle internalization and endosomal escape compared to untargeted LENN, indicating the importance of the clathrin pathway in contributing to the delivery efficiency of LENN. Endocytosis inhibition experiments further support the involvement of the clathrin pathway. These findings highlight the compelling features of LENN with respect to their size, in vitro and in vivo targetability, mRNA encapsulation efficiency, complex stability, gene expression, and "green" manufacturability, offering an attractive alternative to existing methods for gene delivery.

nonviral mRNA delivery system | targeted gene delivery | elastin-like polypeptide | self-assembled mRNA vector | clathrin-mediated endocytosis

Significance

Lipid nanoparticle and viral vectors are the most common mRNA delivery vehicles, however, they can face manufacturing, storage, efficacy, and safety challenges. We introduce layer-by-layer elastin-like polypeptide nucleic acid nanoparticle (LENN), a delivery vehicle formed via self-assembly of elastin-like polypeptides (ELP) and cyclodextrin-polyarginine (CD-PLR_{10}) components that are biorenewable and versatile for nucleic acid delivery. LENN formulations maintain their stability, encapsulation efficiency, excellent in vitro and in vivo performance, while retaining their activity after lyophilization and rehydration. This study reveals how LENN are internalized, highlighting the influence that cellular phospholipid changes have on cargo uptake and delivery. Elucidating these internalization mechanisms could help advance the development of ELP-based delivery systems that offer improved efficacy and precision for targeted gene therapies.

Gene therapy is one of the most promising therapeutic opportunities, with the potential for modulating gene expression to ameliorate a wide variety of human diseases. This powerful approach has been used to prevent and treat various diseases, including cancers, infections, cardiovascular diseases, diabetes, and other unmet medical needs (1). Several gene therapies have received FDA approval, particularly for the treatment of various types of cancer (2). This was achievable due to significant advances in molecular biology, RNA technology, vaccinology, and drug delivery technologies (3). As interest in gene delivery continues to grow, research is increasingly focused on targeting both viral and nonviral vector systems to enhance the delivery of nucleic acids to tumors (4). Viral vectors are favored in some cases due to their high transfection efficiency and their evolved mechanisms of cellular entry and escape, however, they often suffer from issues such as high immunogenicity, limited cargo capacity, and complex production challenges (5–7). Nonviral vectors, by contrast, are comparatively cost-effective, multimodal, and display reduced immunogenicity, but often suffer from low transfection efficiency (7). The initial approval of Onpattro and the fast-track approval of COVID vaccines has brought significant attention to lipid nanoparticles (LNPs) for nucleic acid delivery (8). Despite the promise LNPs hold, there are inherent limitations to this platform, including challenges in manufacturing, long-term storage, cold chain challenges, chemical modification of the nucleic acid cargo (9), crowded intellectual property space (10), high costs, and reliance on synthetic lipid precursors derived from nonbiorenewable sources such as petrochemical feedstocks (11–15). Thus, considerable need and scope remains for developing more manufacturable, biorenewable, adaptable, and effective gene delivery systems.

Our lab recently introduced a **l**ayer-by-layer **e**lastin-like polypeptide (ELP)-based **n**ucleic acid **n**anoparticle (LENN) system that is an agile nonviral vector for targeted nucleic acid delivery that can accommodate varying cargo sizes ranging from siRNA to plasmid constructs. LENN are a promising platform for gene delivery using biorenewable materials

Author contributions: S.D., B.D.E., C.R.F., and D.H.T. designed research; S.D., F.Q., M.H., A.P., B.E., and C.R.F. performed research; S.D., F.Q., C.R.F., and D.H.T. analyzed data; D.H.T. guided research & secured funding; and S.D. and D.H.T. wrote the paper.

Competing interest statement: The ELP purification method by organic solvent extraction has been submitted by Purdue University for patent protection.

This article is a PNAS Direct Submission.

[1]To whom correspondence may be addressed. Email: davethom@purdue.edu.

This article contains supporting information online at https://www.pnas.org/lookup/suppl/doi:10.1073/pnas.2502486122/-/DCSupplemental.

Published January 7, 2026.

that can be manufactured cost-effectively on large scale (16), laying the foundation for an alternative approach to gene delivery that does not require viral vectors, LNP, or chemically modified nucleic acids that may introduce off-target effects and/or safety challenges (9). In addition, ELP-based therapies are anticipated to have good tolerability due to their derivation from human tropoelastin, although direct in vivo evidence of their biodegradability and low immunogenicity remains limited (16–18). The LENN reported here are comprised of three components: 1) ELPs; 2) β-cyclodextrin-polyarginine 10-mer or 5-mer conjugates (CD-PLR_{10} or CD-PLR_5); and 3) firefly luciferase mRNA as the nucleic acid cargo (Scheme 1). The outermost layer of the LENN system is comprised of ELP sequences that have been designed for targeted delivery using $(VPGVG)_{24}$-EGF (V24-EGF) or as an untargeted $(VPGVG)_{40}$ (V40) control. The EGF moiety facilitates selective binding to EGFR overexpressing bladder cancer cells, while the hydrophobic guest residues (valines and prolines) engage in host:guest interactions with the cyclodextrin component that promotes nanoparticle self-assembly (16). The CD-PLR_{10} or CD-PLR_5 plays a dual structural and functional role, wherein the cyclodextrin cavity anchors ELP prosthetic groups in host:guest fashion and the polyarginine segment forms ionomeric complexes with the negatively charged nucleic acid cargo, condensing it into a nanoparticle core. Additionally, the arginine rich segment also plays a pivotal role in facilitating endosomal escape of the nucleic acid cargo following internalization. Finally, firefly luciferase mRNA, a reporter gene, is used as a nucleic acid payload that allows quantitative assessment of transfection and delivery effectiveness within the targeted ceplsl.

Since targeted nanoparticle-mediated gene delivery involves three crucial steps: 1) engagement of specific receptors on the cell surface, 2) internalization via energy-dependent or independent processes, and 3) cargo escape from the endosome (19, 20), understanding the pathway and timescale of the delivery process is essential for optimizing their design and enhancing their therapeutic efficacy (21). Recognition of these challenges motivated this study to provide a better understanding of targeted LENN interactions with epidermal growth factor receptor-positive (EGFR+) bladder tumor cells and evaluate their interactions with LENN. It is known that different endocytic internalization pathways have varying impacts on therapeutic performance (22, 23). Clathrin-mediated endocytosis forms internalizing vesicles via clathrin-coated pits, directing cargo to lysosomal degradation, recycling, or escape (24). Caveolae-mediated endocytosis, on the other hand, involves cholesterol-rich invaginations and often targets organelles like the endoplasmic reticulum (ER). Clathrin- and caveolae-independent pathways, such as flotillin-mediated processes or small GTPases (e.g., Arf6, Cdc42), enable actin-driven internalization. Macropinocytosis, characterized by engulfing extracellular fluid and particles ranging from 0.2 to 5 μm, is initiated by generation of plasma membrane ruffles due to actin polymerization (25, 26). Understanding the pathway(s) utilized by the LENN system is crucial for optimizing its performance. The most widely used techniques for studying intracellular trafficking mechanisms are 1) the use of pharmacological inhibitors to block a particular pathway, 2) gene knockout of a specific internalization pathway target, or 3) labeling of endocytosis vesicles using fluorescent protein fusions for monitoring by confocal microscopy or flow cytometry (19, 27, 28). The role of different proteins involved in endocytosis have been widely studied, but the contribution of plasma membrane lipids in this process are not as fully investigated. Plasma membrane composition changes provide the necessary fluidity and membrane curvature required for the endocytosis process (29–31). Understanding nanoparticle interactions with plasma membranes, intracellular pathways, and cargo release can improve delivery vehicle design. By clarifying each step, it becomes possible to pinpoint bottlenecks and develop strategies to enhance gene delivery efficiency (31, 32).

We report a study that explores the internalization mechanisms of LENN and investigates the critical role of cellular lipid profile changes in cargo uptake and delivery within EGFR+ T24 bladder cancer cells. This deeper understanding may guide the development of next-generation ELP-based delivery platforms that are safer, more efficient, and tailored to specific therapeutic targets.

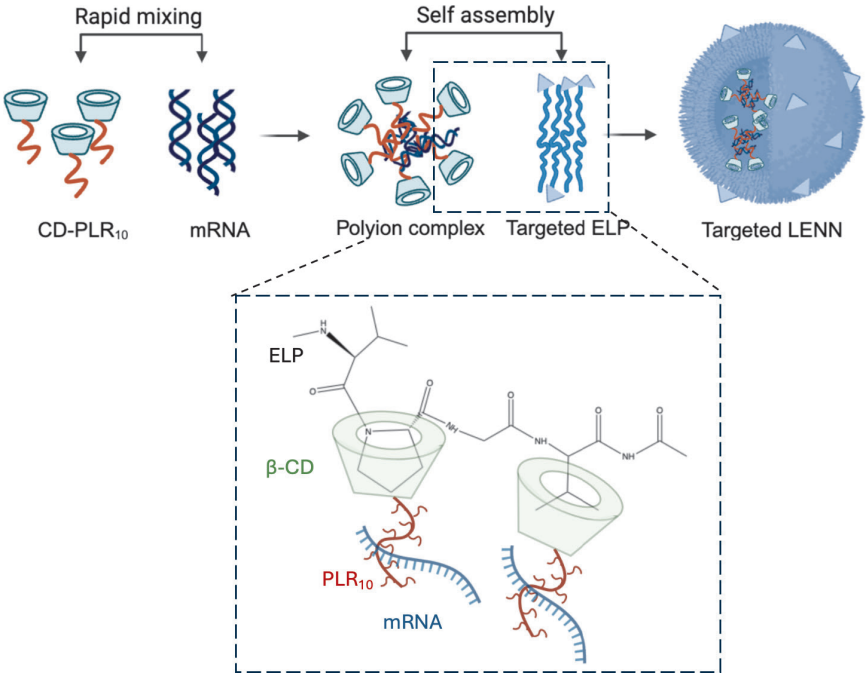

Scheme 1. Conceptual diagram of the initial electrostatic condensation step for mRNA complexation with CD-PLR_{10} followed by ELP coating to form LENN via hydrophobic host:guest interactions between the ELP prosthetic groups and the cyclodextrin cavities.

EGFR-mediated internalization is known to be primarily dependent on clathrin-mediated endocytosis; however, it was not clear whether this internalization mechanism would occur in a multivalent EGFR-targeted LENN system. Our results indicate that EGF-bearing LENN are predominantly internalized through clathrin-mediated endocytosis and localize within endosomal compartments within 1 h of incubation. Target-specific engagement of LENN with EGFR+ bladder tumor cells was observed In vitro and in vivo. Furthermore, in vitro mRNA expression studies indicated that lyophilized LENN stored at −20 °C for 3 d displayed a performance profile similar to freshly prepared LENN solutions. Additionally, lipid profiling analysis revealed that membrane biogenesis, detected as upregulated cellular phospholipid synthesis and acyl chain remodeling, plays a significant role in the mechanism of LENN endocytosis and endosomal trafficking on the 0.5 to 4 h timescale.

Results and Discussion

Structural and Physical Characterization of Polyion Complexes and LENN. Our initial efforts focused on probing the physical characteristics, encapsulation efficiency, stability, and morphology of Polyion complexes, untargeted LENN, and targeted LENN prepared by bulk mixing methods. Our findings show that LENN particle sizes are strongly dependent on precursor solution concentrations. At mRNA concentrations up to 0.05 mg/mL, particle sizes determined by dynamic light scattering (DLS) were found to be ~100 nm for Polyion complexes and about 500 nm for LENN. These data were corroborated by cryoelectron microscopy (Cryo-EM) analysis where aggregates along with isolated complexes were both observed (*SI Appendix*, Fig. S1 *A* and *C*). Furthermore, a study of particle sizes as a function of time indicated that the initially formed ~100 nm Polyion complexes increased to an average diameter of 380 nm within 1 min after V24-EGF addition, indicating a rapid interaction between Polyion particles and ELP that increases LENN diameters over a 30 min period. Particle aggregation was observed at high LENN concentrations, however, upon lowering the formulation concentration to 0.0025 mg/mL mRNA, a significant decrease in size was observed (450 nm → 100 nm) (*SI Appendix*, Fig. S1*B*). Based upon these findings, the 0.0025 mg/mL concentration was used for all subsequent studies.

Average diameters as a function of Nitrogen:Phosphorus ratio (NP) for targeted LENN and Polyion complexes were also determined by DLS. We found that V24-EGF LENN, particularly at the higher NP ratios of NP10 and NP15, exhibit smaller (Fig. 1, diameter) and more uniform particle sizes, as indicated by their lower polydispersity index values (PDI ≤ 0.3). Encapsulation efficiency tests show that the encapsulation performance improved with increasing NP ratio, (Fig. 1, encapsulation efficiency), highlighting the critical role of CD-PLR_{10} in the complexation process. Significant changes in encapsulation efficiencies were observed upon heparin challenge of LENN and Polyion complexes (Fig. 1, encapsulation efficiency). Notably, LENN at NP10 and above maintain their encapsulation efficiency compared to Polyion complexes even after exposure to a heparin challenge, indicating their robustness and potential for reliable delivery of intact mRNA cargo under physiological conditions. Zeta potential measurements (Fig. 1, ζ potential) show that LENN display higher positive surface charges at higher NP, potentially contributing to better colloidal stability and enhanced interactions with negatively charged cellular membranes without promoting instability toward heparin challenge. The increase in ζ potential at higher NP suggests that the ELP layer does not fully mask the Polyion complex

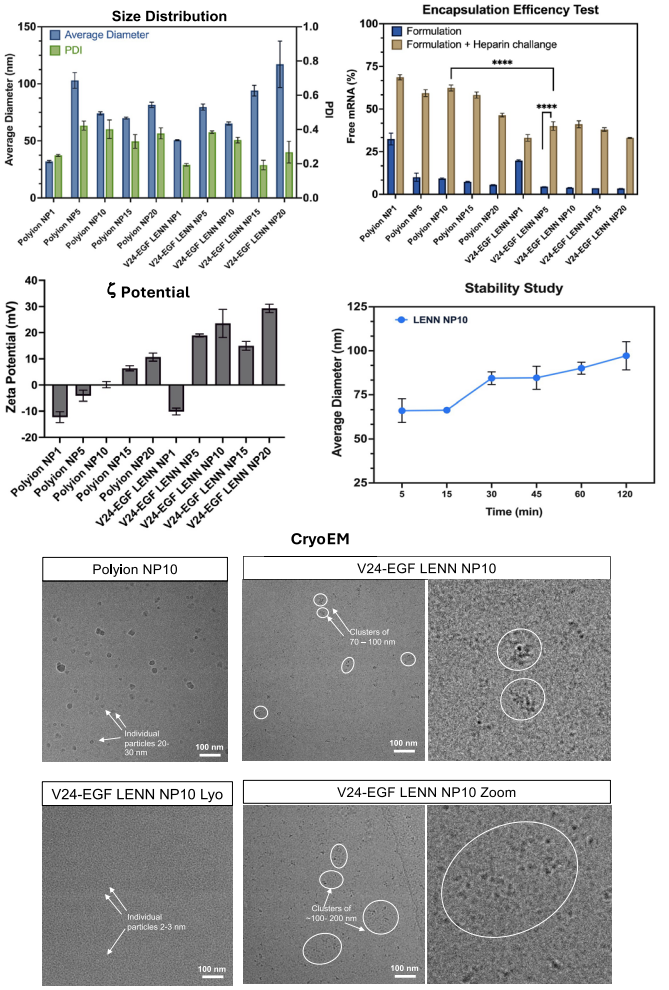

Fig. 1. Characterization of Polyion complexes and LENN formulations. Particle Size: Average hydrodynamic diameter (blue) and polydispersity index (PDI, green) of Polyion and LENN complexes measured by DLS. NP1, NP5, NP10, NP15, NP20 complexes show varying sizes and PDI. Encapsulation Efficiency: Encapsulation efficiency of mRNA in Polyion and LENN complexes before (blue) and after (brown) 5× heparin exposure. LENN formulations show significantly higher stability than Polyion complexes, with LENN NP10 retaining nearly 80% encapsulation efficiency after heparin challenge (****$P < 0.0001$). Statistical differences were calculated using GraphPad Prism v5.0 by ANOVA ($P < 0.05$) using Tukey's multiple comparisons ($P < 0.05$), where *$P < 0.05$, **$P < 0.01$, ***$P < 0.001$, ****$P < 0.0001$. Zeta Potential: The ζ of V24-EGF LENN increases more rapidly with NP ratio than for analogous Polyion complexes. Stability Study: LENN NP10 diameters in water as a function of time show only a modest increase in size up to 120 min. CryoEM Images: CryoEM analysis of Polyion NP10, LENN NP10, and LENN NP10 Lyo (lyophilized) complexes reveal individual particles ranging from 2 to 3 nm for lyophilized particles, and clusters of 100 to 200 nm for LENN NP10. Polyion complexes range in sizes between 20 and 40 nm. (Scale bar, 100 nm.)

core from excess arginine residues, leading to higher apparent surface charge.

Stability studies of LENN NP10 in solution (Fig. 1, cryoEM) indicate that the complexes maintain a diameter between 60 and 95 nm over a 2 h period. CryoEM images revealed that LENN NP10 particles consist of smaller diameter particles (2 to 3 nm) that are clustered into ~70 to 100 nm aggregates that are more uniform compared to the larger and more heterogeneous Polyion NP10 particles (20 to 40 nm). This clustered aggregate appearance and particle heterogeneity is commonly observed in peptide-based formulations; this behavior has previously been overcome by strategies like flow mixing and microfluidics approaches. Most significantly, lyophilization of LENN followed by storage for 3 d at −20 °C and rehydration in water did not alter the LENN NP10

dimensions, where a more uniform distribution of particles with 2 to 3 nm features was observed, suggesting that CD-PLR$_{10}$-based nanoparticles can be effectively lyophilized, stored, and reconstituted without loss of structural integrity. A β-cyclodextrin derivative bearing a shorter polyarginine segment, CD-PLR$_5$, was also tested in a comparative performance study. Particle diameter, ζ potential and encapsulation efficiency measurements revealed smaller sizes (30 to 50 nm), a net negative ζ (−15 mV), and 95% encapsulation efficiency at NP ≥5, however, heparin challenge data showed that CD-PLR$_5$ particle stability was substantially lower than for CD-PLR$_{10}$ complexes of similar CD:ELP ratio (*SI Appendix*, Fig. S2 *A–C*). Furthermore, the LENN formations of CD-PLR$_5$ were observably less stable since their diameters were observed to progressively increase over a 2 h time interval (*SI Appendix*, Fig. S2*D*). Therefore, all subsequent studies were conducted using CD-PLR$_{10}$ based formulations. These results indicate that CD-PLR$_{10}$-based targeted LENN perform better than Polyion complexes of similar NP with respect to diameter uniformity, encapsulation efficiency, stability, and morphology. Based on the favorable properties of LENN NP10, we then tested their potential as an mRNA delivery vehicle.

Determining the Mechanism of LENN Endocytosis. Our prior work demonstrated that V24-EGF can rapidly and specifically engage EGFR+ overexpressing bladder cancer cells, including T24 human bladder tumor cells, compared to control cells with low EGFR expression levels (33). Subsequent studies showed that V24-EGF LENN were capable of targeted delivery of functional siRNA or pDNA, except when in the presence of a large excess of free EGF that suppressed targeted LENN activity due to EGFR blockade (16). To further test the scope and mechanism of nucleic acid delivery in this system, we prepared LENN using Cy5.5-V24-EGF (31) and MFP-488-labeled mRNA for monitoring LENN uptake and intracellular distribution by confocal microscopy. Fig. 2*A* compares EGFR+ T24 cells treated for 1 h with 1) V24-EGF LENN complexes, 2) V24-EGF LENN complexes + excess free EGF (receptor blockade), and 3) Polyion complexes. V24-EGF LENN treatment in the absence of free EGF produced strong intracellular MFP-488 and Cy5.5 fluorescence, indicative of efficient cellular uptake and internalization of V24-EGF LENN. In contrast, free EGF blockade caused significant reduction in MPF-488 and Cy5.5 fluorescence, indicating the importance of unoccupied EGFR for V24-EGF LENN binding and endocytosis by T24 cells. Interestingly, Polyion complexes yielded punctate MPF-488 fluorescence throughout the cell interior.

The effects of specific endocytosis inhibitors on V24-EGF LENN NP uptake were then investigated to further probe the potential roles of any internalization pathways involved. Treatment with filipin, a caveolae-mediated endocytosis inhibitor (32), at increasing concentrations (1.5 to 10.0 μM) showed no dose-dependent reduction in ELP or mRNA signal within EGFR+ T24 cells (Fig. 2*B*), suggesting that V24-EGF LENN complexes do not utilize caveolae-mediated

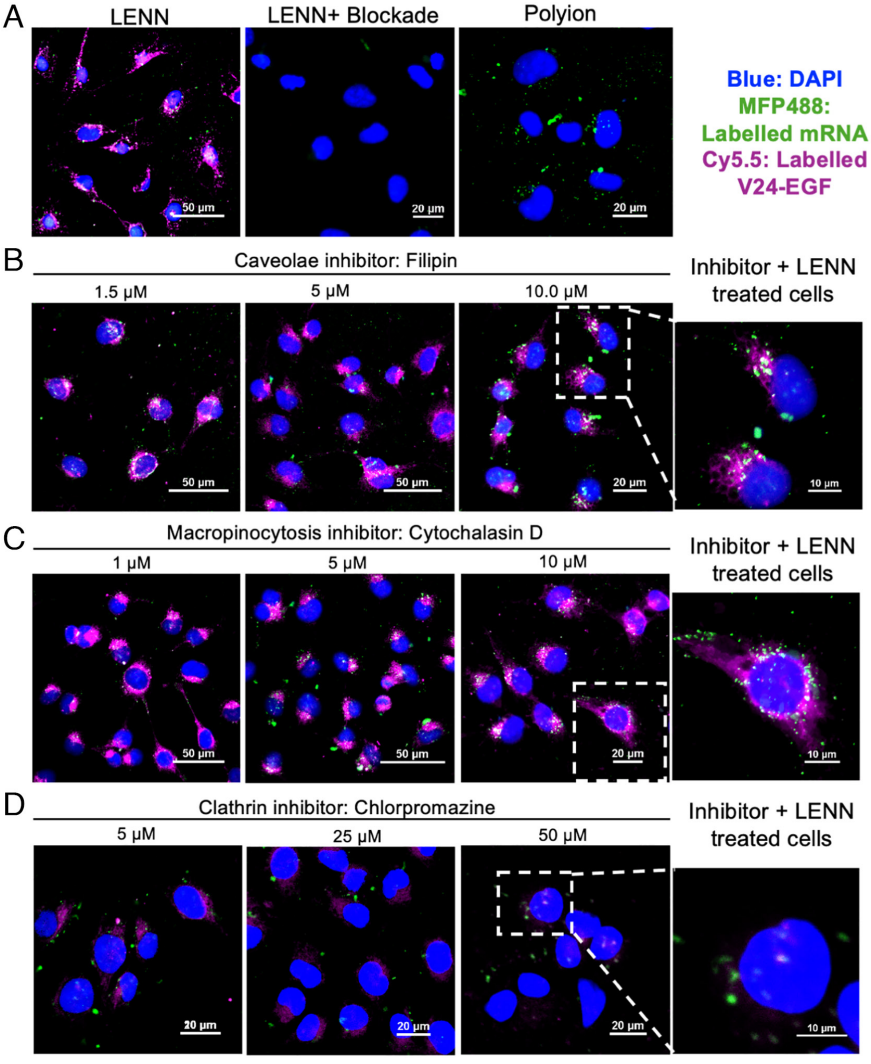

Fig. 2. Confocal microscopy analysis of LENN cellular uptake pathways in T24 cells probed using endocytosis inhibitors. All inhibitors were tested, by incubating with T24 cells 30 min before LENN treatment. Confocal microscopy images showing the uptake of labeled mRNA (green, MFP488) and V24-EGF (magenta, Cy5.5), where nuclei are stained with DAPI (blue). (*A*) Inhibitor-free treatments: T24 cells treated with LENN (*Left*), LENN with EGF receptor blockade (*Middle*), and Polyion complexes (*Right*). (*B*) Caveolae inhibitor (filipin): Treatment with filipin (1.5 to 10.0 μM) in LENN-treated cells. (*C*) Macropinocytosis inhibitor (Cytochalasin D): Cytochalasin D (1.0 to 10.0 μM). (*D*) Clathrin inhibitor (chlorpromazine): Increasing concentrations of chlorpromazine (5.0 to 50.0 μM) gradually diminish cellular uptake of LENN. Higher magnification images shown in the right column are for each treatment condition at the highest concentration tested. (Scale bar, 10 to 50 μm.)

pathways for cellular entry. Inhibition of the micropinocytosis pathway with Cytochalasin D (34) reveals a similar trend—at concentrations from 1 to 10 μM, there is no noticeable decrease in nanoparticle internalization, with significant intracellular MPF-488 and Cy5.5 fluorescence signals observed (Fig. 2*C*)—suggesting that macropinocytosis does not contribute to the uptake of V24-EGF LENN complexes. When the cells were treated with the clathrin-mediated endocytosis inhibitor chlorpromazine (34) at concentrations from 5 to 50 μM, a dramatic decrease in intracellular MPF-488 and Cy5.5 fluorescence was observed after incubation with V24-EGF LENN complexes (Fig. 2*D*). The progressive reduction of fluorescence with increasing chlorpromazine concentration is a strong indicator of the critical role that clathrin-mediated endocytosis plays in the internalization process of V24-EGF LENN complexes. Taken together, these results suggest that V24-EGF LENN complexes are internalized primarily through clathrin-mediated endocytosis. An important outcome of these findings is the recognition that the constitutive clathrin-mediated endocytosis pathway that is known for monomeric EGF uptake via EGFR engagement (35) is not altered by LENN that are studded with multiple copies of EGF on their surface. This contrasts with findings in endothelial cells, where monomeric antibodies targeting CAMs like PECAM-1 and ICAM-1 are poorly internalized, yet multivalent carriers targeting these molecules trigger a distinct, rapid endocytic process (36, 37), illustrating how multivalent ligand presentation can alter uptake pathways. In our case, however, the multivalent display of EGF on LENN does not appear to induce an alternative mechanism, rather it continues to rely on the classical clathrin-mediated endocytosis pathway that is typical for monomeric EGF, highlighting how endocytic responses to multivalency are context-dependent and shaped by the specific receptor–ligand system.

We also infer from the observation of punctate MPF-488 fluorescence in T24 cells treated with Polyion complexes that these particles are likely entering via nonspecific adsorptive endocytosis pathways after binding of the positively charged particles to negatively charged plasma membrane constituents.

Flow cytometry studies were performed under similar conditions to quantify the effect of different inhibitors for internalization. The results demonstrate that clathrin-mediated endocytosis plays a significant role in LENN uptake, especially for mRNA internalization (Fig. 3*B*). Chlorpromazine reduced the percentage of mRNA-MFP488- and ELP-Cy5.5-positive cells, with high chlorpromazine concentrations reducing mRNA internalization to just 5.0% and ELP uptake to 66.3%. Even at medium chlorpromazine concentrations, the mRNA uptake dropped to 5.8%, supporting the involvement of clathrin in mRNA delivery (Fig. 3*D*). This substantial inhibition suggests that clathrin-coated pits are crucial for efficient entry of targeted LENN. Furthermore, the targeted LENN retained high uptake in cells without inhibitor treatment (95.2% for ELP and 58.6% for mRNA, Fig. 3 *A* and *B*). Macropinocytosis and caveolae-mediated endocytosis, inhibited by cytochalasin D and filipin, respectively, had smaller impacts on uptake (Fig. 3 *A* and *B*). Reduction in mRNA and ELP signal intensities were observed for both cytochalasin D and filipin at their highest concentrations. These reductions suggest that alternative mechanisms may be engaged in LENN uptake, however, they are modest compared to the clathrin-mediated endocytosis pathway for mRNA delivery by EGF LENN. These data suggest that LENN formulations rely heavily on clathrin-mediated endocytosis, with minor contributions from other endocytic pathways.

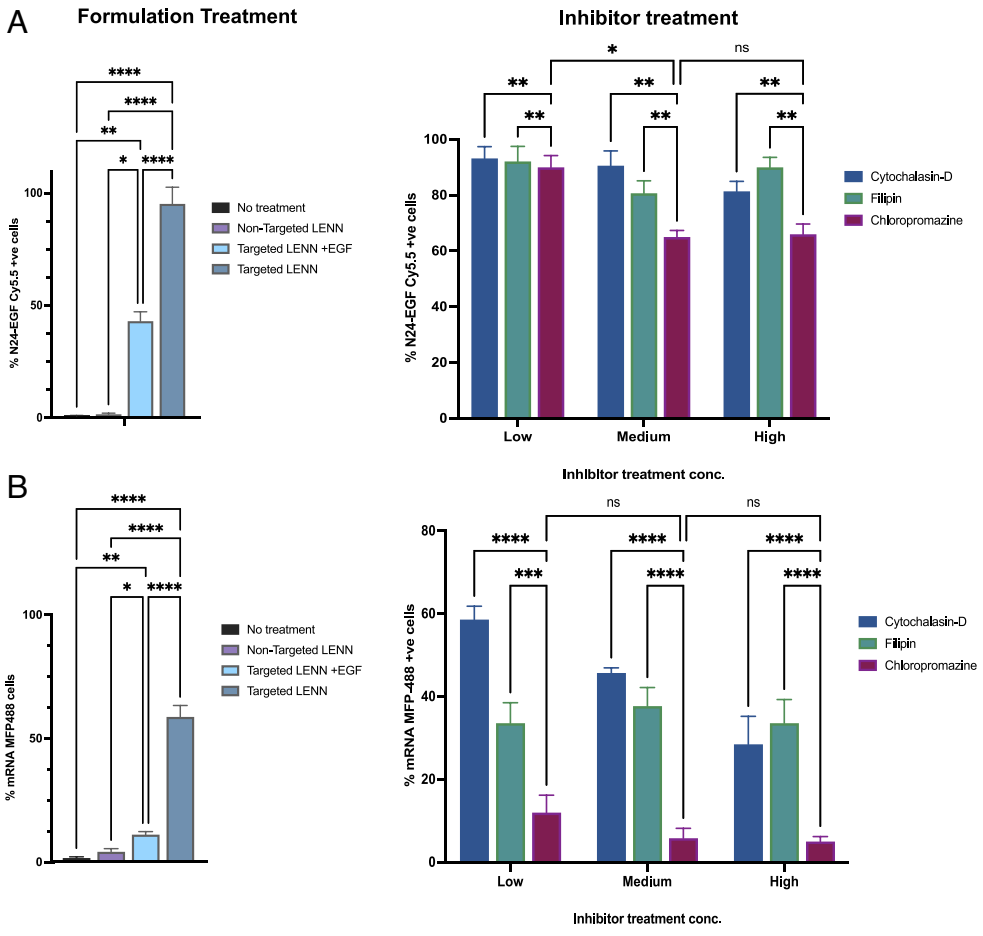

Fig. 3. Flow cytometry analysis of cellular uptake and endocytosis of targeted LENN formulations in T24 cells. *Left*: Percentage of V24-EGF-Cy5.5-positive cells (*A*) and % mRNA MFP-488 positive cells (*B*) after treatment with non-targeted LENN, targeted LENN with free EGF, and targeted LENN. *Right*: Targeted LENN uptake pattern after treatment by cytochalasin D, filipin, and chlorpromazine at various concentrations with cell-associated fluorescence signals measured for (*A*) V24-EGF-Cy5.5-positive cells and (*B*) % mRNA MFP-488 positive cells. The cells were monitored on flow cytometry using the 488 and 640 nm channels. Statistical differences were calculated using GraphPad Prism v5.0 by ANOVA ($P < 0.05$) using Tukey's multiple comparisons ($P < 0.05$), where ns = 0.1234, *$P < 0.0332$, **$P < 0.0021$, ***$P < 0.0002$, ****$P < 0.0001$.

Performance of LENN In Vitro and In Vivo. Our next effort focused on understanding the internalization rate of V24-EGF LENN complexes. Confocal microscopy images of T24 cells collected 0, 1, and 4 h after a 1 h exposure to V24-EGF LENN complexes are shown in Fig. 4*A*. Immediately after removing the LENN formulation and rinsing the cells with PBS (t = 0 h), the majority of cells at 0 h displayed large vesicular structures where the colocalized fluorescence from both Cy5.5-V24-EGF and MPF-488-mRNA appear in endo-lysosomal compartments (Fig. 4*A* and *SI Appendix*, Fig. S4), indicating that the complexes were internalized and trafficking through the endosomal pathway during the 1 h incubation period. It is noteworthy that the MPF-488 fluorescence was more dispersed than the Cy5.5 signal, suggesting that the mRNA had already begun to decomplex and escape the endosomal compartment, however, there were still regions of fluorescence signal overlap that are indicative of endosomal entrapment. After 4 h, most of the MPF-488-mRNA signal appears diffuse, suggesting successful escape from the endosome, however, some colocalization within the endo-lysosome compartment remains (Fig. 4 and *SI Appendix*, Fig. S4).

The encouraging findings from the endosomal escape studies motivated us to evaluate the potential of LENN for targeted Fluc mRNA delivery and luciferase gene expression. The luminescence data in Fig. 4*B* demonstrate that V24-EGF LENN formulations, particularly at NP10 and NP15, achieve significantly higher luciferase activities than no treatment controls and similar activity to Polyion complexes that enter via nonspecific adsorptive internalization pathways. We conclude from these findings that V24-EGF LENN complexes are capable of target-specific cellular uptake and endosomal escape to enable robust mRNA expression postinternalization.

A major challenge confronting LNP delivery systems is the physical and chemical lability (38) of their liquid formulations that necessitate a −80 °C cold chain to retain their bioactivity (39). As an initial test to probe the storage stability of LENN, we tested the effect of lyophilization on mRNA expression. Surprisingly, there was no significant loss in expression efficiency for V24-EGF LENN NP10 that were stabilized with 10% glycerol, lyophilized, stored as a dry powder for 3 d at −20 °C, and rehydrated in 400 µL H_2O relative to freshly prepared V24-EGF LENN NP10 solutions (Fig. 4*C*). It is interesting to note that V24-EGF LENN samples that were lyophilized with 10% DMSO as cryoprotectant had similar luciferase activities to those of fresh Polyion solutions. Even though lyophilization appears to increase their diameters, these findings suggest that EGF-containing LENN retain their functionality (*SI Appendix*, Fig. S3).

Standard of care for non-muscle-invasive bladder cancer treatment relies on intravesical instillation of Bacillus Calmette Guerin or mitomycin C, however, these approaches often face limitations due to short in-dwell times within the bladder lumen and the presence of a glycosaminoglycan (GAG) layer that limits access to the bladder epithelium. Tumor growth is often accompanied by disruption of the GAG layer in the tumor environment, creating an opportunity for enhanced engagement of therapeutic agents with exposed tumor cells (40). To assess this potential, we evaluated the targeted vs. nontargeted LENN in vivo over the 1 h dwell time that is typical for intravesical administrations. Using V24-EGF

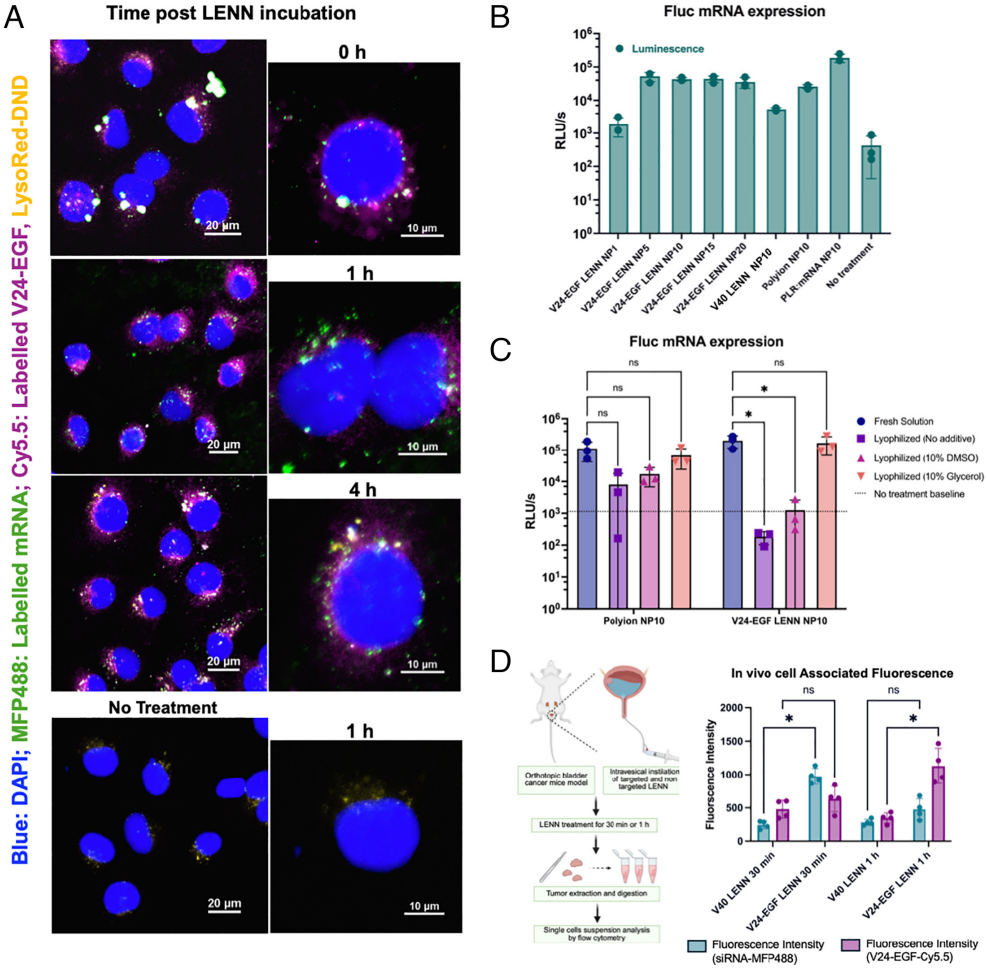

Fig. 4. Analysis of mRNA delivery and expression in T24 cells treated with LENN formulations. (*A*) Confocal microscopy of intracellular mRNA and ELP localization: Cells treated with LENN formulation show time-dependent localization of fluorescently labeled mRNA (green, MFP488) and ELP/V24-EGF (magenta, Cy5.5). Lysosomes were stained with LysoRed-DND (yellow) to track mRNA/ELP colocalization. (Scale bar, 10 to 20 µm.) (*B*) Luciferase mRNA expression assay: Luminescence measurements (RLUs) demonstrate successful transfection of Fluc mRNA across various LENN and Polyion formulations. (*C*) Effect of lyophilization on Fluc mRNA expression: Comparison of luciferase expression in cells treated with fresh or lyophilized LENN and Polyion NP10 formulations. Anything above the line is a positive signal. (*D*) Schematic representation of in vivo workflow and assessment of cell-associated fluorescence: Fluorescence intensity of siRNA (MFP488) and ELP (Cy5.5) after administration of LENN formulations in vivo. Targeted LENN formulations show significantly higher cell-associated fluorescence than untargeted LENN at 1 h, indicating efficient delivery of siRNA and ELP. Statistical analysis was done using GraphPad Prism v5.0 by ANOVA ($P < 0.05$) using Tukey's multiple comparisons ($P < 0.05$), where $^*P < 0.05$, $^{**}P < 0.01$, $^{***}P < 0.001$, $^{****}P < 0.0001$.

LENN labeled with MPF-488-siRNA and Cy5.5-V24-EGF or Cy5.5-V40, MB49 orthotopic tumor-bearing mice were treated by intravesical infusion of LENN for 30 min and 1 h, followed by exhaustive rinsing with PBS. After euthanasia in accordance with current IACUC guidelines, the tumors were excised, digested with accumax, and analyzed by flow cytometry for MPF-488 and Cy5.5 signal intensity. Tumors exposed to V24-EGF LENN complexes exhibited significantly higher MPF-488 fluorescence intensity at 30 min with a slight decrease at 1 h, presumably due to quick cytosolic siRNA processing. Cy5.5 fluorescence intensity progressively increased between 30 min and 1 h due to continued binding and internalization of the EGF-targeted complexes. Tumors from V40 LENN-treated animals had lower MPF-488 and Cy5.5 fluorescence at both time points, thus highlighting the importance of targeting for enhanced delivery efficiency (Fig. 4*D*). These findings highlight the efficiency of V24-EGF LENN to overcome some of the key delivery challenges in vivo for rapid and targeted nucleic acid therapeutic agent delivery in very aggressive tumors by demonstrating both successful engagement and the internalization of the targeted particles within the tumor environment. With further mouse model studies and more uniform formulation preparation, future investigations will focus on biodistribution, PK/PD analysis, and therapeutic efficacy to establish the translational potential of this platform.

Lipid Profiling Analysis of T24 Cells Treated with LENN Formulations: Additional Insights Into the Endocytosis Mechanism. The plasma membrane plays a critical role in the receptor-mediated internalization mechanism by continuously generating intracellular vesicles that undergo invagination, scission, and fusion with other organelles. By regulating the proportion of different lipid classes, their acyl chain composition, degree of unsaturation, and lateral heterogeneity, the lipid membrane species must continuously adapt to changing extracellular signals and transmembrane flux of constituents. Phospholipids, the predominant class of lipids in the plasma membrane, are key components responsible for maintaining membrane plasticity (41).

To provide additional insight into the uptake and escape pathway for the mRNA cargo of LENN, we pursued a lipid profiling study of T24 cells treated for 1 h with V24-EGF LENN, V40 LENN, and Polyion complexes while monitoring their impact on different lipid classes (*SI Appendix*, Figs. S5 and S9). Multiple time points were tested to understand the endocytosis pathway and the role that different lipids may play in this dynamic process. The most significant differences were observed in the phosphatidylcholine (PC), phosphatidylinositol (PI), and sphingomyelin (SM) classes of lipids in cells treated with each of the formulations, while the targeted LENN preparations also showed a significant difference in phosphatidylethanolamine (PE), phosphatidylserine (PS),

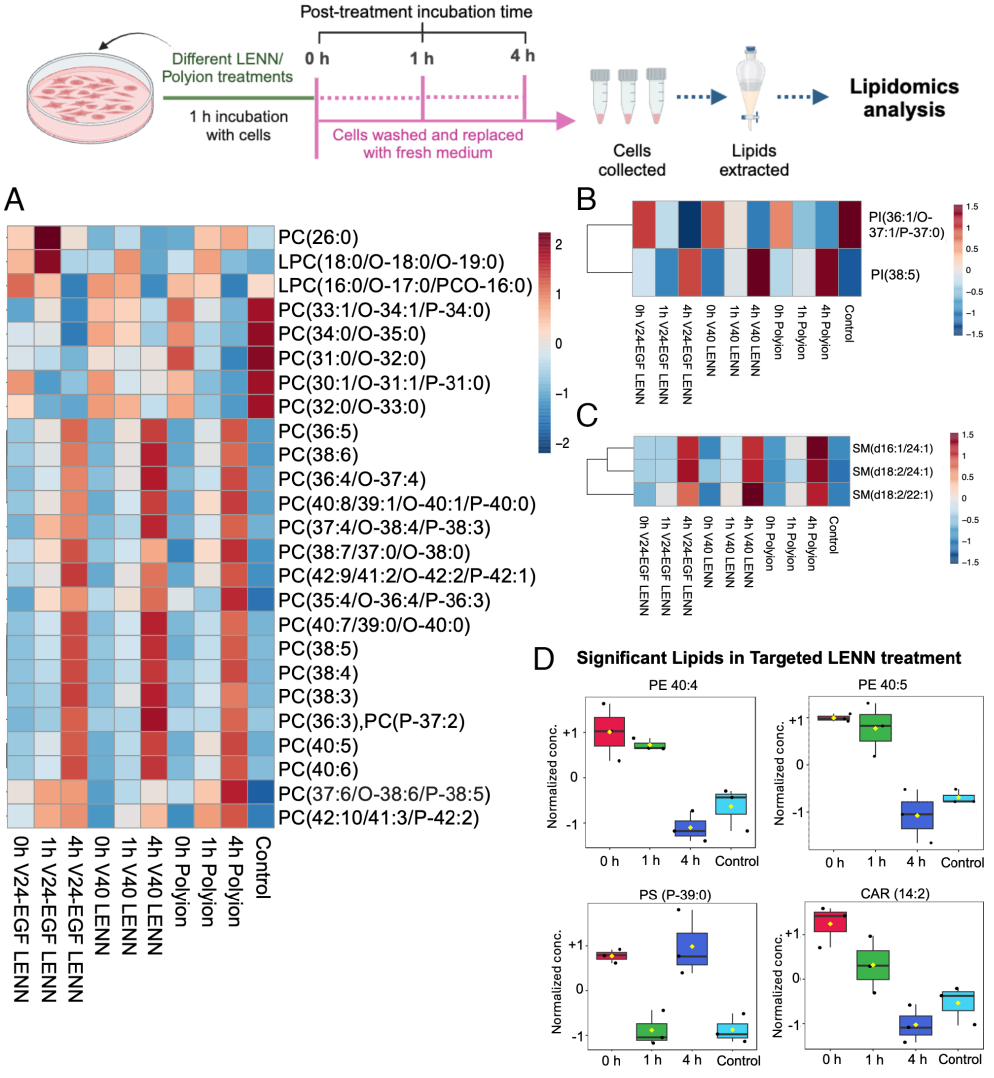

Fig. 5. Lipidomic analysis of T24 cells treated with V24-EGF LENN, V40 LENN, and Polyion complexes at multiple time points (0, 1, and 4 h). Phosphatidylcholine (PC), lysophosphatidylcholine (LPC), phosphatidylinositol (PI), and sphingomyelin (SM) species are shown. (*A*) Heatmap of normalized PC and LPC intensities, with red indicating higher and blue indicating lower lipid concentrations. (*B*) Heatmaps of PI and SM species, showing time-dependent changes in PI (38:5) and PI (36:1/O-37:1/P-37:0), as well as SM (d18:1/24:1), SM (d18:2/24:1), and SM (d18:2/22:1). (*C*) Boxplots of significant lipids identified in the targeted V24-EGF LENN treatment, including PE (40:4), PE (40:5), PS (P-39:0), and carnitine (CAR 14:2), illustrating time-dependent changes in lipid levels at 0, 1, and 4 h. (*D*) The four plots compare how the abundance of specific lipid species changes over time following LENN treatment, relative to control. Lipids showed higher normalized levels at 0-1 h and a decrease by 4 h, suggesting a time-dependent lipid class-specific dynamic response. All the results were analyzed by MetaboAnalyst software and normalized by ANOVA analysis P value < 0.05.

and tetradecadienoylcarnitine (CAR) species. An increase in unsaturated PC lipids, accompanied by a decrease in saturated PC, was observed over time from 0 h to 4 h for each of the different formulations compared to no treatment controls (Fig. 5*A*). Lysophosphatidylcholine (LPC) (18:0) was also significantly elevated after 1 h in the V24-EGF LENN samples compared to other treatments. An increase in PI (38:5) over time was observed for all formulations, while PI (36:1/O-37:1/P-37:0) decreased (Fig. 5*B*). Elevated sphingomyelin (SM) content was also observed for all treatments at longer incubation time points (Fig. 5*C*). Changes in these lipid profiles—particularly the increase in unsaturated acyl chain content and the enrichment in lipid classes associated with increasing membrane curvature—are indicative of a dynamic reorganization of the cellular lipids during the endocytosis process over the course of the 4 h monitoring period. PC, known to contribute significantly to the regulation of membrane fluidity (42), was observed to increase in the degree of unsaturated acyl chains, with an accompanying decrease in saturated and monounsaturated PC species. These changes contribute to increased membrane fluidity (43) that is essential during endocytosis events. Furthermore, prior efforts to investigate the dependence of PC composition on clathrin-mediated endocytosis showed that an increase in LPC (18:0) content contributes to a disordered lipid phase. The conical shape factor of LPC is crucial for inducing membrane curvature on the outer monolayer to facilitate early invagination of the plasma membrane (44). Our lipid composition data suggests an important role for LPC (18:0) in modulating clathrin-dependent endocytosis and initial vesicle formation. PI also contributes to enhancing membrane dynamics. For example, PI lipids act as precursors for phosphoinositol phosphates that play an important role in the early-to-late endosomal formation process. A specific PI, phosphatidylinositol 4,5-bisphosphate (PI (4,5) P2), is observed to be essential for clathrin-coated pit formation (45–47). Our data show that PI (36:1/O-37:1/P-37:0) decreases across treatments, while PI (38:5) increases—further indicating the importance of lipid chain unsaturation in contributing to membrane fluidity. Across the 4 h analysis period, the levels of different SM species were observed to increase. Sphingolipids function as secondary messengers for intracellular and extracellular signaling. Sphingomyelins are also known to be involved in asymmetric lipid raft formation along with cholesterol in cellular membranes (48, 49). Since clathrin-mediated endocytosis is typically not dependent on lipid raft formation, the SM increase may indicate a stimulation of intracellular communication pathways, as the intensity of different SM species peaked at the 4-h time point in all treatment conditions.

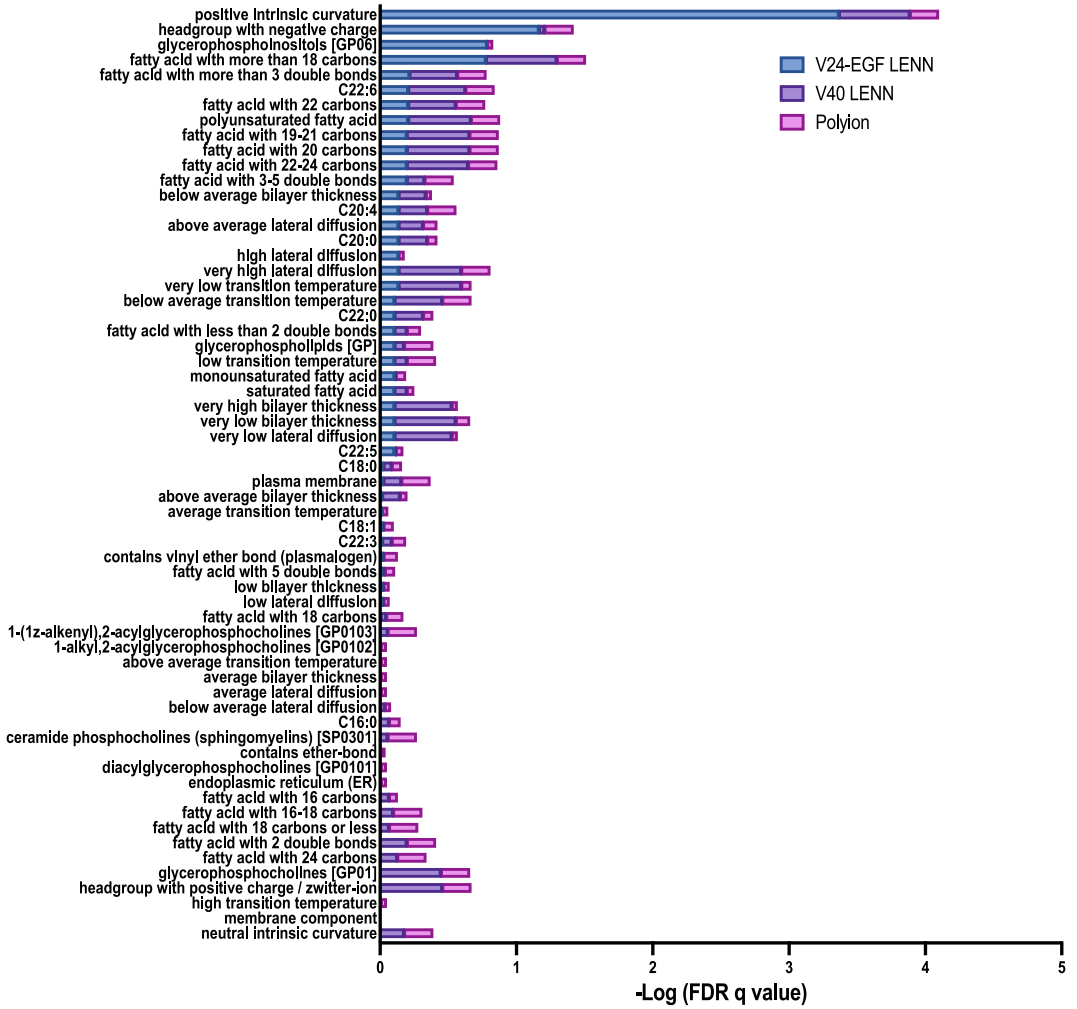

Fig. 6. Lipid ontology enrichment analysis of lipid profiling dataset using the LION/web tool. The bar graph illustrates significantly enriched lipid-associated biophysical and cellular features/functions (e.g., fatty acid chain length, saturation, intrinsic curvature, lateral diffusion, bilayer thickness, and organelle localization). The −log(FDR q-value) represents the statistical significance of enrichment for each term. This analysis provides insight into the functional lipid landscape and potential biological implications of lipid alterations in N24-EGF LENN, N40 LENN, and Polyion complexes at 1 h compared to no treatment group.

An interesting observation from this study was that only the targeted LENN treatment had notable increases for lipid classes such as PS, PE, and tetradecadienoylcarnitine. The time-dependent increase of PS at 0 h after LENN treatment, followed by a decrease at 1 h and then a rise again at 4 h (Fig. 5*D*), suggests that PS may be playing multiple roles in the endocytosis pathway. PS, a type of negatively charged glycerophospholipid found in the inner leaflet of the plasma membrane, is known to stimulate membrane curvature and promote endocytic invagination and vesicle fission during clathrin-mediated endocytosis. It is also present during early and late endosomal phases of the endocytosis process (50–52). Our data indicates that PS may be contributing to the initial invagination and early endosomal process for V24-EGF LENN endocytosis, while the decrease at 1 h would be consistent with endosomal escape of the LENN cargo. The decrease in PS at 1 h suggests a higher processing rate of PS that is likely involved in the escape mechanism. The rise at 4 h is consistent with PS species playing a role in the late endosomal phase. Two different species of PE (40:4 and 40:5) showed increases at 0 and 1 h, followed by a drop at 4 h (Fig. 5*D*). PE, an ionizable lipid, induces membrane tension, has intrinsic fusogenic properties, and is implicated in enhancing endosomal escape (53, 54). Our results suggest elevated levels of PE at 0 and 1 h, pointing to its role in inducing membrane curvature and, more importantly, its part in the endosomal escape process by improving the fusogenic ability of LENN complexes with the endosomal membrane. Last, carnitines (CARs) were observed to be elevated at 0 h compared to the no treatment group followed by a relative decrease in their concentration. Carnitines have no known correlation with endocytosis mechanisms, but they are involved in transfer of long chain fatty acids for β-oxidation (55). Elevation of CAR(14:2) may be reflective of the high degree of lipid reorganization in the cell, with CAR(14:2) serving to regulate the high number of acyl chains as the cell tries to sustain transacylation flux during endocytosis.

Lipid Ontology enrichment analysis (56) was used to profile lipid structural and functional remodeling across three conditions: V24-EGF LENN, V40 LENN, and Polyion complexes at the 0 h timepoint (Fig. 6). The analysis revealed distinct enrichment patterns in membrane biophysical properties, fatty acid composition, and subcellular localization, indicating condition-specific membrane adaptation. V24-EGF LENN–treated cells exhibited the strongest enrichment for positive intrinsic curvature, a biophysical trait that facilitates membrane bending, vesicle formation, and endocytosis (57). Additionally, there was a relative increase in negatively charged headgroup lipids and lipids associated with the ER, suggesting active trafficking and ER remodeling (*SI Appendix*, Fig. S10). Enrichment of both saturated fatty acids (e.g., C16:0, C22:0) and polyunsaturated fatty acids (PUFAs) (e.g., C22:5, C22:6) indicates a delicate balance between membrane-ordering and fluidizing forces, potentially to maintain curvature stress while enabling dynamic vesicular processes. In comparison, the V40 LENN condition showed a modest adaptation in lipid profile favoring membrane fluidity and curvature adaptability, with enrichment of highly unsaturated fatty acids (e.g., C22:6, C20:4), very high lateral diffusion, and moderate positive intrinsic curvature (Fig. 6 and *SI Appendix*, Fig. S11). The presence of plasmalogen-containing lipids further supports an adaptive, antioxidant response, likely enabling signal transduction and homeostatic flexibility (58). Polyion complex-treated cells demonstrated enrichment in ether-linked phospholipids, monounsaturated fatty acids, and plasma membrane-localized lipids, accompanied by average bilayer thickness and moderate lateral diffusion components (Fig. 6 and *SI Appendix*, Fig. S12). These characteristics suggest surface-level membrane remodeling—likely due to nanoparticle interaction—without strong perturbation of internal membrane dynamics or stress responses, implying a neutral, homeostatic adaptation. Overall, the lipid profiling data analysis points toward a very dynamic membrane reorganization with little evidence of any inflammatory/anti-inflammatory pathway activation. To further evaluate lipid remodeling over time, we examined the degree of unsaturation in phosphatidylcholine (PC) species (*SI Appendix*, Fig. S13). Across all treatment groups, we observed a time-dependent increase in polyunsaturated PCs (≥3 double bonds), with the most significant increases at the 4-h timepoint. Importantly, cells treated with V24-EGF LENN and V40 LENN both showed comparable levels of PUFA-enriched PCs at 4 h, suggesting that both conditions promote membrane fluidity through PUFA incorporation. Polyion complex treatment also led to increased unsaturation over time, reinforcing its role in membrane reorganization.

Although our dataset does not include direct measurements of cytokines or inflammatory signaling pathways, the lipid profiles allow indirect inference regarding the inflammatory potential of the treatments. Across all conditions, saturated and unsaturated fatty acid levels remained relatively balanced, with a progressive increase in unsaturation over time, suggesting a general trend toward membrane fluidity and adaptation, rather than proinflammatory lipid accumulation. Overall, our results suggest that poly-arginine-based nanoparticles induce balanced membrane adaptation without triggering inflammatory lipid signatures, supporting their potential as immuno-compatible delivery systems.

Taken together, the lipid profiling data corroborate our confocal microscopy findings. At 0 h, endosome formation and colocalization of the mRNA and the V24-EGF signals was observed, followed by more dispersed signals at 1 h and decreased fluorescence intensity at 4 h. Notably, lipid species involved in clathrin-mediated endocytosis and endosomal escape (PS and PE species) were not significantly elevated in either V40 LENN or the Polyion complex–treated cells. These endosomal processing observations are consistent with the more robust performance of targeted V24-EGF LENN, where clathrin-mediated endocytosis facilitates a rapid and direct internalization mechanism followed by successful endosomal escape. These findings align with the luminescence data, where cells treated with the Polyion complexes and V40 LENN showed lower luminescence intensity than V24-EGF LENN formulations (Fig. 4*B*). Overall, these results suggest the onset of the early endosomal phase at 0 h for targeted LENN, followed by the endosomal escape mechanism observable at 1 h, and then late endosome processing and receptor recycling at 4 h.

Conclusion

Viral vector-based therapies are the most common approach for gene delivery, accounting for approximately 70% of clinical trials of nucleic acid–based therapeutic candidates. Lipid-based nonviral vector-based alternatives offer greater formulation flexibility, however, they often fail to perform effectively due to challenges like liver tropism and the endosomal escape bottleneck (59). This study introduces the LENN system as a promising alternative to viral and LNP gene delivery methods. LENN formulations were found to display promising encapsulation efficiency, stability, and gene expression properties. LENN retain their functionality even after lyophilization, making them a promising mRNA vector system for therapeutic applications that require long-term storage. The EGF ligand employed in this study conferred enhanced target specificity and internalization efficiency of targeted LENN relative to untargeted LENN and Polyion complexes. EGF LENN were found to predominantly enter T24 cells via the clathrin-mediated endocytosis pathway on the basis of receptor blockade and endocytosis inhibitor experiments (Fig. 7).

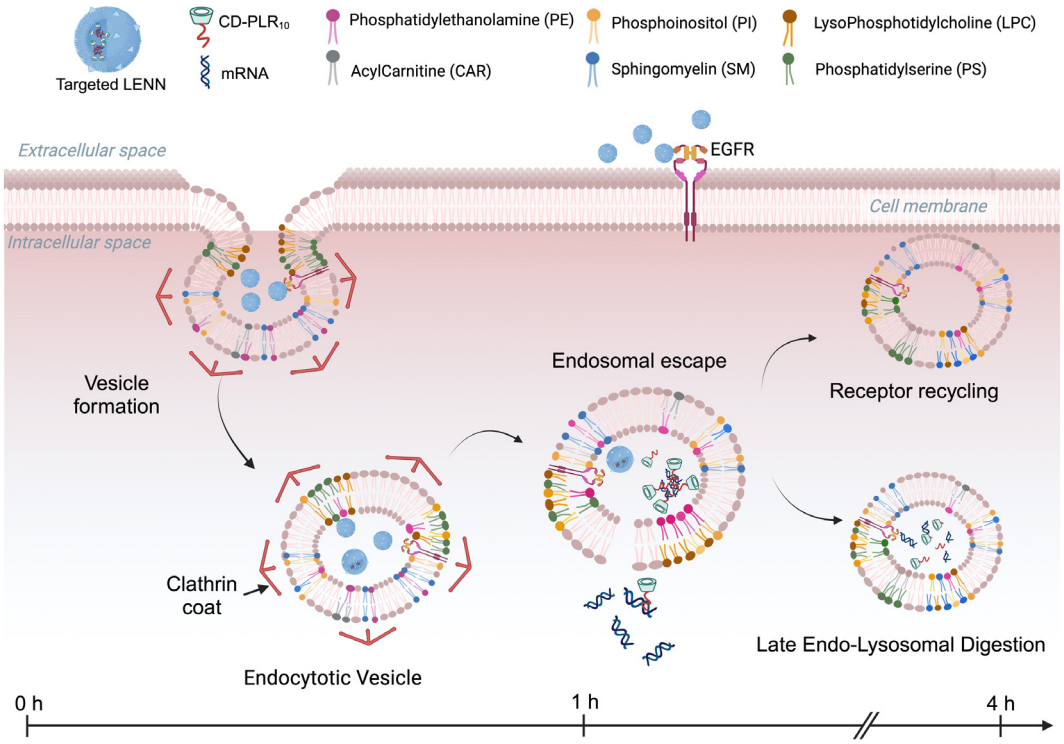

Fig. 7. Conceptual diagram of the endocytosis mechanism and endosomal escape of V24-EGF LENN mRNA cargo in T24 bladder cancer cells. Created in BioRender [S. Darji (2021), BioRender.com/t03v298].

Additionally, this work highlights the involvement of phospholipids like PS and PE in early endosomal invagination and escape, thus emphasizing the importance of understanding the interactions between delivery systems and the cellular lipid environment. The LENN system presents a versatile and scalable approach to nonviral gene delivery using biomanufacturable materials and enabling the −20 °C storage of lyophilized single vial powders for rehydration before use. Taken together, these data demonstrate the excellent uptake, stability, and mRNA expression efficiency of V24-EGF LENN in vitro and in vivo and highlight the potential of V24-EGF LENN as a versatile and efficient delivery system for mRNA therapeutics. Further investigation into optimizing lyophilization conditions and exploring the mechanisms underlying the enhanced expression of targeted LENN will be crucial for advancing this technology toward clinical applications.

Materials and Methods

Synthesis and Characterization of LENN Nanoparticles. LENN were synthesized by combining ELP with CD-PLR_{10} in a layer-by-layer assembly. The following stocks were prepared: nucleic acid cargo (mRNA) in RNAase-/LPS-free water (0.1 mg/mL) and polycation (CD-PLR_{10} or CD-PLR_5) in H_2O as 1 mM stock. Nucleic acid and polycations were vortex-mixed for 30 s at the desired N:P ratio followed by V24-EGF (targeted) or V40 (untargeted) ELP addition to form LENN. ELP were added in 1 molar excess of valine + proline residues relative CD-PLR_{10}. The final concentrations were adjusted according to the experimental requirements. DLS and zeta potential measurements were performed using a Zetasizer Nano ZS (Malvern Instruments) to determine particle size, polydispersity index (PDI), and surface charge. Cryo-EM was used to visualize the morphology and structural integrity of the nanoparticles.

Synthesis of CD-PLR_5 and CD-PLR_{10}. The pentaarginine or decaarginine precursor (1 equiv) was treated with 1,1′-carbonyldiimidazole (1 to 2 equiv) and stirred for 6 h in a 2:1 THF:DMF solvent mixture under Ar at 20 °C. 6-Deoxy-6-amino-β-cyclodextrin (1.1 to 3 equiv) was then added and the mixture stirred at 20 °C for 8 h. The reaction mixture was then transferred to a 100 to 500 Da MWCO dialysis cell to remove unreacted CDI and imidazole side products. After dialysis, the materials were lyophilized to yield a white solid.

DLS. The particle size, size distribution, and ζ potential of the various formulations were analyzed using a Malvern Zetasizer Nano ZS. LENN were prepared using 1 μg of nucleic acids encapsulated in either Polyion complexes or LENN, with a final dilution with 400 μL of a RNAase free water. All measurements were conducted in triplicate to ensure accuracy and reproducibility.

Encapsulation Efficiency. Encapsulation efficiency of the mRNA into LENN was determined by fluorescence spectroscopy. After the formation of nanoparticles, the free mRNA was detected using a QuantIT kit according to the manufacturer's instructions. For stability challenge, heparin was added at a final conc of 0.1 mg/mL and incubated for 10 min before adding the QuantIT reagents. The fluorescence was finally measured at λ_{ex} 480, λ_{em} 520 nm.

Cryo-EM. All the samples were prepared using 1 μg of nucleic acid with a final dilution using 400 μL RNAase free water. Concentrated formulations were diluted to a 50 μL volume before analysis. The Cryo-EM imaging experiments were performed by the Purdue University Cryo-EM facility.

Stability Study of Lyophilized Samples. To assess stability of lyophilized formulations, LENN were prepared as mentioned above followed by addition of 10% v/v DMSO or glycerol and initially frozen at −20 °C, followed by cooling to −80 °C and lyophilization overnight. After storage of the lyophilized powders at −20 °C for 3 d, sample rehydration was performed to give the same 2.5 μg/mL concentration and formulations tested for structural integrity and encapsulation efficiency compared to fresh samples following the procedure above.

Cell Culture. T24 bladder cancer cells were cultured in DMEM supplemented with 10% FBS at 37 °C in a humidified atmosphere containing 5% CO_2. Cells were seeded at a density of 2×10^5 cells per well in 6-well plates and allowed to grow to 80% confluence before treatment with LENN.

Cellular Uptake and Endocytosis Studies. LENN were labeled with Cy5.5 for tracking ELP and MFP-488 for mRNA. To determine the pathway of cellular uptake, cells were pretreated with inhibitors specific for different endocytic pathways:

chlorpromazine (5 to 50 μM) for clathrin-mediated endocytosis, filipin (1.5 to 10 μM) for caveolae-mediated endocytosis, and cytochalasin D (1 to 10 μM) for macropinocytosis. After 30 min of inhibitor incubation, cells were treated with LENN and incubated for 1 h at 37 °C. Cellular uptake was assessed using confocal microscopy and quantified via flow cytometry. For endo-lysosomal tracking studies, the cells were incubated with LysoRed DND for 40 min before analysis. Cells were fixed with 2% paraformaldehyde before analysis. Note: Cytochalasin D and filipin treatments displayed signs of cell death around 25 μM and 10 μM concentrations, respectively; chlorpromazine cell death was observed at 50 μM.

Gene Expression Studies. Luciferase mRNA transfection was performed to assess the gene delivery efficiency of LENN. Cells were treated with LENN containing luciferase mRNA for 1 h, followed by removal of media and addition of fresh DMEM. After 24 h, luciferase activity was measured using the Luciferase Assay System (Promega) and quantified in relative light units (RLU) using a luminometer. Results were normalized to total protein content measured by 260/280 nm.

In Vivo Tumor Targeting Studies. To conduct in vivo studies, Hif-1α siRNA was labeled using the MFP-488 Label IT® kit, while Cy5.5 was utilized for labeling both V24-EGF and V40. The Label IT® reagent covalently labels nucleic acids through a three-part system: a label (e.g., fluorophore) for detection, a linker that electrostatically associates with the negatively charged nucleic acid backbone, and a reactive alkylating group that forms a stable covalent bond with nucleophilic sites on the nucleic acid. This covalent labeling occurs without disrupting the nucleic acid structure or its hybridization capability. NHS-ester dyes, such as NHS-Cy5.5, label proteins, or peptides by targeting primary amine groups, typically found on the N terminus. In slightly basic conditions (pH 7.2 to 8.5), the primary amine forms a stable covalent amide bond while releasing N-hydroxysuccinimide as a byproduct.

Formulations of siRNA-MFP488 and CD-PLR were prepared by combining them in an NP4 ratio to create the Polyion complexes, followed by complexation with 10x V24-EGF-Cy5.5/V40-Cy5.5 to form LENN. All LENN formulations were tested on 8- to 10-wk-old female C57BL/6 mice at an siRNA dose of 6.6 μg/mL. Orthotopic MB49 tumors were established by single point cauterization using a Bovie Derm 101 on maximum setting with a Kirschner 34 Ga wire inserted at the bladder dome via Surflo 24 Ga x ¾″ catheter, followed by instillation of 1 x 10^5 cells and outgrowth for 5 days before treatment. In vivo studies were conducted in four groups: a) V24-EGF LENN for 30 min, b) V40 LENN for 30 min, c) V24-EGF LENN for 1 h, and d) V40 LENN for 1 h, with each test group consisting of 4 mice. Initially, mice were anesthetized and their bladders emptied, followed by catheter insertion and incubation with different LENN formulations for 30 min or 1 h. Subsequently, the bladder was washed three times with 4 M urea PBS after the incubation period. Mice were then euthanized, the bladder resected, and then bivalved for imaging using a Spectral Ami device configured to detect Cy5.5 and MFP-488 emission. Isolated tumors were then digested to single cells using accumax solution for approximately 2 to 3 h, and the solution was filtered through a 70 μm sieve. The cells were centrifuged, and the pellet was resuspended using FACS buffer for analysis using a BD Fortessa cytometer. Data were collected for siRNA-MFP488 and Cy5.5-labeled V24-EGF/V40 and analyzed using FSC express.

Lipid Profiling Analysis. For lipid profiling analysis, 250 k cells/well were seeded and kept in 37 °C, 5% CO_2 until 80% confluence was achieved. Subsequently, cells were treated with either V24-EGF LENN, V40 LENN, or Polyion complexes for 1 h, followed by incubation for 0, 1, and 4 h. All conditions used formulations at NP10 using 0.5 mg/mL mRNA per well. After incubation, the medium was removed, and the cells washed with 1× PBS, followed by harvesting and centrifugation (2,000×*g* for 10 min) for lipid extraction using the Bligh & Dyer method. (60) Briefly, 200 μL of water was added to the cell pellet and vortexed to promote cell lysis. Then, 550 mL of methanol and 250 mL chloroform (HPLC grade, chilled to −20 °C) was added and the solution vortexed, followed by incubation at 4 °C for 15 min. Later, another 250 μL water and 250 μL chloroform were added, allowing the solution to become biphasic. Samples were centrifuged for 10 min at 5,000×*g* and the bottom layer was transferred to a new microtube followed by SpeedVac evaporation. For analysis, the samples were resuspended in 200 μL of injection solvent (3:6.65:0.35 ACN:MeOH:300 mM NH_4OAc). For each run, samples were diluted by 50× in injection solvent and analyzed by MRM profiling for 1.5 h using an Agilent 6410 QQQ using methods described previously (61, 62). MetaboAnalyst 6.0 software was used to quantify the relative amounts of the lipid species and the data analyzed using univariate and statistical analysis, as well as cluster analysis with heat map. Lipid profiling data were normalized using autoscaling to obtain a normal distribution. ANOVA $P < 0.05$ was used. Only the significant lipid species were represented in Fig. 5, while *SI Appendix* has all other species that were screened, but not significant. This data is publicly available at: https://purr.purdue.edu/publications/5016/1.

Statistical Analysis. All experiments were performed in triplicate unless stated otherwise. Data were expressed as mean ± SD. Statistical significance was determined using one-way ANOVA followed by Tukey's multiple comparisons test, with *P*-values < 0.05 considered significant. GraphPad Prism v5.0 was used for statistical analysis.

Data, Materials, and Software Availability. All study data are included in the article and/or *SI Appendix*.

ACKNOWLEDGMENTS. We thank the Purdue Institute for Cancer Research NCI Cancer Center Support Grant (CA23168) and the Graduate Research Fellowship program for financial support of this project. Additional support of this effort by the Flow Cytometry Shared Resource, Chemistry Research Instrumentation Center, Cryoelectron Microscopy Facility, Metabolite Profiling Facility, and Biological Evaluation Shared Resource is gratefully acknowledged.

Author affiliations: [a]Department of Chemistry, Multidisciplinary Cancer Research Facility, Purdue University, West Lafayette, IN 47907; [b]Bindley Bioscience Center, Purdue University, West Lafayette, IN 47907; and [c]Department of Comparative Pathobiology, Multidisciplinary Cancer Research Facility, Purdue University, West Lafayette, IN 47907

1. B. B. Mendes *et al.*, Nanodelivery of nucleic acids. *Nat. Rev. Methods Primers* **2**, 24 (2022).
2. D. Chancellor, D. Barrett, L. Nguyen-Jatkoe, S. Millington, F. Eckhardt, The state of cell and gene therapy in 2023. *Mol. Ther.* **31**, 3376–3388 (2023).
3. S. Shetty, P. C. Alvarado, D. Pettie, J. H. Collier, Next-generation vaccine development with nanomaterials: Recent advances, possibilities, and challenges. *Annu. Rev. Biomed. Eng.* **26**, 273–306 (2024).
4. D. M. Dogbey *et al.*, Technological advances in the use of viral and non-viral vectors for delivering genetic and non-genetic cargos for cancer therapy. *Drug Deliv. Transl. Res.* **13**, 2719–2738 (2023).
5. S. Miron-Barroso, E. B. Domenech, S. Trigueros, Nanotechnology-based strategies to overcome current barriers in gene delivery. *Int. J. Mol. Sci.* **22**, 8537 (2021).
6. B. Lu *et al.*, The next-generation DNA vaccine platforms and delivery systems: Advances, challenges and prospects. *Front. Immunol.* **15**, 1332939 (2024).
7. M. H. Butt *et al.*, Appraisal for the potential of viral and nonviral vectors in gene therapy: A review. *Genes* **13**, 1370 (2022).
8. Y. Yan *et al.*, Non-viral vectors for RNA delivery. *J. Control. Release.* **342**, 241–279 (2022).
9. F. Cheng *et al.*, Research advances on the stability of mRNA vaccines. *Viruses* **15**, 668 (2023).
10. C. Hald. Albertsen *et al.*, The role of lipid components in lipid nanoparticles for vaccines and gene therapy. *Adv. Drug Deliv. Rev.* **188**, 114416 (2022).
11. H. Daraee, A. Etemadi, M. Kouhi, S. Alimirzalu, A. Akbarzadeh, Application of liposomes in medicine and drug delivery. *Artif. Cells Nanomed. Biotechnol.* **44**, 381–391 (2016).
12. G. Aquino-Jarquin, The patent dispute over the breakthrough mRNA technology. *Front. Bioeng. Biotechnol.* **10**, 1049873 (2022).
13. Y. Eygeris, M. Gupta, J. Kim, G. Sahay, Chemistry of lipid nanoparticles for RNA delivery. *Acc. Chem. Res.* **55**, 2–12 (2022).
14. M. Cerone, T. K. Smith, A brief journey into the history of and future sources and uses of fatty acids. *Front. Nutr.* **8**, 570401 (2021).
15. Z. He, Z. Liu, Y. Chen, Chemical design strategy of ionizable lipids for in vivo mRNA delivery. *ChemMedChem* **19**, e202400199 (2024).
16. A. Aayush, S. Darji, K. M. Estes, E. Yeh, D. H. Thompson, Development of an elastin-like polypeptide-based nucleic acid delivery system targeted to EGFR+ bladder cancer cells using a layer-by-layer approach. *Biomacromolecules* **25**, 5729–5744 (2024).
17. F. S. Nouri, X. Wang, X. Chen, A. Hatefi, Reducing the visibility of the vector/DNA nanocomplexes to the immune system by elastin-like peptides. *Pharm. Res.* **32**, 3018–3028 (2015).
18. M. Shah *et al.*, Biodegradation of elastin-like polypeptide nanoparticles. *Protein Sci.* **21**, 743–750 (2012).
19. J. J. Rennick, A. P. R. Johnston, R. G. Parton, Key principles and methods for studying the endocytosis of biological and nanoparticle therapeutics. *Nat. Nanotechnol.* **16**, 266–276 (2021).
20. D. Manzanares, V. Cena, Endocytosis: The nanoparticle and submicron nanocompounds gateway into the cell. *Pharmaceutics* **12**, 371 (2020).
21. S. Xiang, X. Zhang, "Cellular uptake mechanism of non-viral gene delivery and means for improving transfection efficiency" in *Gene Therapy - Tools and Potential Applications*, F. Martín-Molina, Ed. (InTechOpen, 2012), p. 756.
22. S. Barua, S. Mitragotri, Challenges associated with penetration of nanoparticles across cell and tissue barriers: A review of current status and future prospects. *Nano Today* **9**, 223–243 (2014).

23. S. E. Gratton *et al.*, The effect of particle design on cellular internalization pathways. *Proc. Natl. Acad. Sci. U.S.A.* **105**, 11613–11618 (2008).
24. M. Kaksonen, A. Roux, Mechanisms of clathrin-mediated endocytosis. *Nat. Rev. Mol. Cell Biol.* **19**, 313–326 (2018).
25. S. D. Conner, S. L. Schmid, Regulated portals of entry into the cell. *Nature* **422**, 37–44 (2003).
26. I. Ruseska, A. Zimmer, Internalization mechanisms of cell-penetrating peptides. *Beilstein J. Nanotechnol.* **11**, 101–123 (2020).
27. Y. Ju, H. Guo, M. Edman, S. F. Hamm-Alvarez, Application of advances in endocytosis and membrane trafficking to drug delivery. *Adv. Drug Deliv. Rev.* **157**, 118–141 (2020).
28. S. Patel *et al.*, Brief update on endocytosis of nanomedicines. *Adv. Drug Deliv. Rev.* **144**, 90–111 (2019).
29. M. Bohdanowicz, S. Grinstein, Role of phospholipids in endocytosis, phagocytosis, and macropinocytosis. *Physiol. Rev.* **93**, 69–106 (2013).
30. H. Ewers, A. Helenius, Lipid-mediated endocytosis. *Cold Spring Harb. Perspect. Biol.* **3**, a004721 (2011).
31. N. Desai *et al.*, Achieving endo/lysosomal escape using smart nanosystems for efficient cellular delivery. *Molecules* **29**, 3131 (2024).
32. T. B. Gandek, L. Koog, A. Nagelkerke, A comparison of cellular uptake mechanisms, delivery efficacy, and intracellular fate between liposomes and extracellular vesicles. *Adv. Healthc. Mater.* **12**, e2300319 (2023).
33. A. Aayush *et al.*, Targeted elastin-like polypeptide fusion protein for near-infrared imaging of human and canine urothelial carcinoma. *Oncotarget* **13**, 1004–1016 (2022).
34. M. Itagaki, Y. Nasu, C. Sugiyama, I. Nakase, N. Kamei, A universal method to analyze cellular internalization mechanisms via endocytosis without non-specific cross-effects. *FASEB J.* **37**, e22764 (2023).
35. Y. Zhou, H. Sakurai, New trend in ligand-induced EGFR trafficking: A dual-mode clathrin-mediated endocytosis model. *J. Proteomics* **255**, 104503 (2022).
36. H. Parhiz *et al.*, Pecam-1 directed re-targeting of exogenous mRNA providing two orders of magnitude enhancement of vascular delivery and expression in lungs independent of apolipoprotein E-mediated uptake. *J. Control. Release.* **291**, 106–115 (2018).
37. V. V. Shuvaev *et al.*, Size and targeting to PECAM vs ICAM control endothelial delivery, internalization and protective effect of multimolecular SOD conjugates. *J. Control. Release* **234**, 115–123 (2016).
38. M. Mehta *et al.*, Lipid-based nanoparticles for drug/gene delivery: An overview of the production techniques and difficulties encountered in their industrial development. *ACS Mater. Au* **3**, 600–619 (2023).
39. X. P. Lin, J. D. Mintern, P. A. Gleeson, Macropinocytosis in different cell types: Similarities and differences. *Membranes* **10**, 177 (2020).
40. F. Qu, S. Darji, D. H. Thompson, Recent advances in drug delivery strategies for high-risk BCG-unresponsive non-muscle invasive bladder cancer: A brief review from 2018 to 2024. *Pharmaceutics* **16**, 1154 (2024).
41. S. Ghadami, K. Dellinger, The lipid composition of extracellular vesicles: Applications in diagnostics and therapeutic delivery. *Front. Mol. Biosci.* **10**, 1198044 (2023).
42. R. F. Saito, L. N. S. Andrade, S. O. Bustos, R. Chammas, Phosphatidylcholine-derived lipid mediators: The crosstalk between cancer cells and immune cells. *Front. Immunol.* **13**, 768606 (2022).
43. S. Ballweg *et al.*, Regulation of lipid saturation without sensing membrane fluidity. *Nat. Commun.* **11**, 756 (2020).
44. I. Ailte *et al.*, Exogenous lysophospholipids with large head groups perturb clathrin-mediated endocytosis. *Traffic* **18**, 176–191 (2017).
45. Y. Posor, W. Jang, V. Haucke, Phosphoinositides as membrane organizers. *Nat. Rev. Mol. Cell Biol.* **23**, 797–816 (2022).
46. G. R. V. Hammond, J. E. Burke, Novel roles of phosphoinositides in signaling, lipid transport, and disease. *Curr. Opin. Cell Biol.* **63**, 57–67 (2020).
47. C. Bissig, S. Johnson, J. Gruenberg, Studying lipids involved in the endosomal pathway. *Methods Cell Biol.* **108**, 19–46 (2012).
48. M. Koivusalo, M. Jansen, P. Somerharju, E. Ikonen, Endocytic trafficking of sphingomyelin depends on its acyl chain length. *Mol. Biol. Cell* **18**, 5113–5123 (2007).
49. M. Lee, S. Y. Lee, Y. S. Bae, Functional roles of sphingolipids in immunity and their implication in disease. *Exp. Mol. Med.* **55**, 1110–1130 (2023).
50. K. Varga, Z. J. Jiang, L. W. Gong, Phosphatidylserine is critical for vesicle fission during clathrin-mediated endocytosis. *J. Neurochem.* **152**, 48–60 (2020).
51. J. Hasegawa *et al.*, A role of phosphatidylserine in the function of recycling endosomes. *Front. Cell Dev. Biol.* **9**, 783857 (2021).
52. T. Hirama *et al.*, Membrane curvature induced by proximity of anionic phospholipids can initiate endocytosis. *Nat. Commun.* **8**, 1393 (2017).
53. E. Alvarez-Benedicto *et al.*, Optimization of phospholipid chemistry for improved lipid nanoparticle (LNP) delivery of messenger RNA (mRNA). *Biomater. Sci.* **10**, 549–559 (2022).
54. D. J. Brock, H. M. Kondow-McConaghy, E. C. Hager, J. P. Pellois, Endosomal escape and cytosolic penetration of macromolecules mediated by synthetic delivery agents. *Bioconjug. Chem.* **30**, 293–304 (2019).
55. N. Longo, M. Frigeni, M. Pasquali, Carnitine transport and fatty acid oxidation. *Biochim. Biophys. Acta* **1863**, 2422–2435 (2016).
56. M. R. Molenaar *et al.*, LION/web: A web-based ontology enrichment tool for lipidomic data analysis. *Gigascience* **8**, giz061 (2019).
57. H. T. McMahon, E. Boucrot, Membrane curvature at a glance. *J. Cell Sci.* **128**, 1065–1070 (2015).
58. Z. A. Almsherqi, Potential role of plasmalogens in the modulation of biomembrane morphology. *Front. Cell Dev. Biol.* **9**, 673917 (2021).
59. I. M. S. Degors, C. Wang, Z. U. Rehman, I. S. Zuhorn, Carriers break barriers in drug delivery: Endocytosis and endosomal escape of gene delivery vectors. *Acc. Chem. Res.* **52**, 1750–1760 (2019).
60. E. G. Bligh, W. J. Dyer, A rapid method of total lipid extraction and purification. *Can. J. Biochem. Physiol.* **37**, 911–917 (1959).
61. L. G. Reis, T. M. Casey, T. J. P. Sobreira, B. R. Cooper, C. R. Ferreira, Step-by-step approach to build multiple reaction monitoring (MRM) profiling instrument acquisition methods for class-based lipid exploratory analysis by mass spectrometry. *J. Biomol. Tech.* **34**, 3fc1f5fe.1972c438 (2023).
62. Z. Xie, C. R. Ferreira, A. A. Virequ, R. G. Cooks, Multiple reaction monitoring profiling (MRM profiling): Small molecule exploratory analysis guided by chemical functionality. *Chem. Phys. Lipids* **235**, 105048 (2021).